PROBLEMY MECHATRONIKI
UZBROJENIE, LOTNICTWO, INŻYNIERIA BEZPIECZEŃSTWA

ISSN 2081-5891

10, 1 (35), 2019, 75-90

PROBLEMS OF MECHATRONICS
ARMAMENT, AVIATION, SAFETY ENGINEERING

Artillery-Missile System Control Under Disturbances Conditions Using a Modified Computed Torque Control Method

Piotr SZMIDT

Kielce University of Technology, Faculty of Mechatronics and Mechanical Engineering,
7 Tysiąclecia Państwa Polskiego Av., 25-314 Kielce, Poland
Author's e-mail address and ORCID:
pszmidt@tu.kielce.pl; https://orcid.org/0000-0002-8488-5277

Received by the editorial staff on 13 April 2018
The reviewed and verified version was received on 19 February 2019

DOI 10.5604/01.3001.0013.0798

Abstract. The paper addresses the issue of remote control of a artillery-missile system when the system is affected by dynamic and kinematic disturbances. The dynamic disturbances analysed in the paper includes disturbances from shots fired while kinematic disturbances are excitation related to the motion of the base on which the system is installed. The object of the study is a system model based on the ZU-23-2MR artillery-missile system produced and operated in Poland, designed to combat lightly armoured air, naval and ground targets. Once the system model and the assumed disturbance types are discussed, further in the paper the system control in azimuth and elevation angular position is analysed. Computed torque control with additional corrective components is presented. A certain inertia in system drive models is also adopted.

This work has been compiled from the paper presented during the 12nd International Armament Conference on *Scientific Aspects of Armament & Safety Technology*, Jachranka, Poland, October 17-20, 2018.

Additionally, uncertainty of model identification is assumed, i.e. object control parameters are different from the parameters of the model which serves as basis for calculating the control parameters. Differences in weights, mass moments of inertia and friction torques arising in the system's drive elements are taken into account. The last part of the paper includes an analysis of the speed of target interception and precision of tracking a manoeuvring aerial target with the interference affecting the system. It was assumed that the system is located on a ship, therefore kinematic disturbances are related to the ship's movement on the sea waves, as well as dynamic disturbances are related to firing the weapon. All simulations were performed in the Scilab environment for a non-linear model of the system. Essential results are shown in a graphical form.
Keywords: automatics and robotics, control, artillery-missile system, inverse dynamics, disturbances

1. INTRODUCTION

The modern tendency to limit human work and replace it with automated systems applies to virtually all areas of life, in particular to dangerous fields, including those related to defence. The driving force related to defence is the constant need to improve safety and reduce the workload of weapons (including artillery) operators to reduce the costs of operation and improving fire accuracy under threat. Within the field of automation and autonomous of gun systems in Poland, the currently conducted work related to the 35 mm AM-35 Tryton gun is worthy of note [1], [2]. There is also an indication that similar work will be done on the naval ZU-23-2MR system [3].

This paper focuses on analysing the controls of the ZU-23-2MR artillery-missile system, taking into account dynamic (weapons fire) and kinematic (weapon base movement) disturbances. This system is manufactured in Poland based on the popular twin-linked 23 mm gun and is frequently fitted with two GROM missiles. The system is intended to combat lightly armoured aerial, naval and ground targets. The gun is characterised by a horizontal range of 3 km, a vertical range of 2 km, and a practical rate of fire of 400 rounds per minute [4].

2. MODEL OF THE STUDY OBJECT

2.1. CAD model

Based on available data, a three-dimensional model of the ZU-23-2MR system was constructed in the SolidWorks software (Fig. 1). This model, based on the geometry of elements and on defined materials, enabled the physical parameters such as masses and mass moments of inertia of individual elements to be estimated.

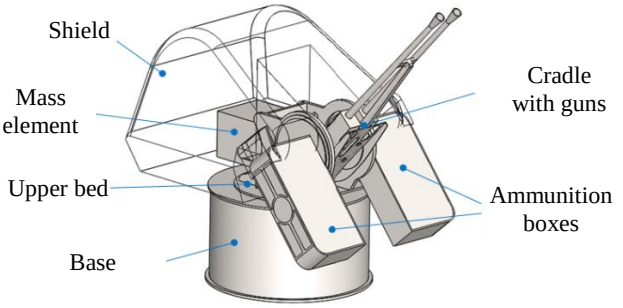

Fig. 1. Model of the system, built in CAD software

Setting the azimuth angle is the responsibility of the rotating upper bed installed on the base, where the other elements shown in Fig. 1 are located. The elevation angle, on the other hand, is set by the motion of the gun cradle relative to the upper mount. Figure 2 shows a diagram of the physical model with important values indicated, which are explained below the figure.

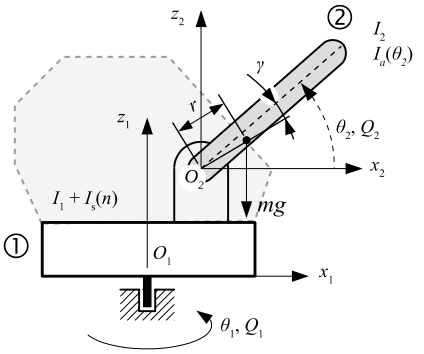

Fig. 2. Physical model diagram

Key to Fig. 2: θ_1 – azimuth angle, θ_2 – elevation angle, Q_1 – general torque affecting the traverse system, Q_2 – general torque affecting the elevation system, I_1 – constant mass moment of inertia of the turret; $pn + q$ – variable mass moment of inertia of the turret depending on the number of bullets in the boxes n; I_2 – constant mass moment of inertia of the gun cradle relative to the elevation rotation axis; $I_a(\theta_2) = a\theta_2^3 + b\theta_2^2 + c\theta_2 + d$ – variable mass moment of inertia of the gun cradle relative to the elevation rotation axis, depending on the elevation angle; m – mass of cradle, including guns; g – gravity acceleration; r – distance of the gun cradle centre of mass from the elevation rotation axis; γ – angular displacement of the gun cradle centre of mass relative to the barrel axis.

2.2. Mathematical model

The mathematical model of system motion dynamics was derived based on the system shown in Fig. 2 and on Lagrange equations of the second kind. For the purpose of numerical simulation and analysis, as well as control selection, a state space representation is more convenient. Two differential equations of the second order, obtained from the Lagrange equations, were therefore written as a system of four differential equations of the first order (1)-(4). $\mathbf{x} = [x_1, x_2, x_3, x_4]^{\mathrm{T}} = [\theta_1, \dot{\theta}_1, \theta_2, \dot{\theta}_2]^{\mathrm{T}}$ was adopted as the state vector; therefore, the azimuth angle, azimuth displacement angular speed, elevation angle and elevation displacement angular speed constitute the system state.

$$\dot{x}_1 = x_2 \tag{1}$$

$$\dot{x}_2 = \frac{-(3ax_3^2 + 2bx_3 + c)x_2x_4 - t_{11}x_2^3 - t_{12}x_2}{I_1 + pn + q + ax_3^3 + bx_3^2 + cx_3 + d} + \frac{M_1 + Z_1}{I_1 + pn + q + ax_3^3 + bx_3^2 + cx_3 + d} \tag{2}$$

$$\dot{x}_3 = x_4 \tag{3}$$

$$\dot{x}_4 = \frac{0{,}5(3ax_3^2 + 2bx_3 + c)x_2^2 - t_{21}x_4^3 - t_{22}x_4 - I_2[\ddot{\tau}_x \sin x_1 + \ddot{\tau}_y \cos x_1]}{I_2} + \frac{-mgr\cos(x_3 + \gamma + \tau_x \sin x_1 + \tau_y \cos x_1) + M_2 + Z_2}{I_2} \tag{4}$$

where: M_1 and M_2 – driving torques forming at reducer output, affecting the motion system in azimuth and elevation, respectively, Z_1 and Z_2 – transient disturbances (moments of force) related to firing, τ_x, τ_y – angular displacement of the system based, t_{11}, t_{12}, t_{21}, t_{22} – coefficients of non-linear approximation of friction functions in joints [5].

3. SYSTEM CONTROL

3.1. General structure of the system

A general flowchart of the system is shown in Fig. 3. Starting with the left side of the figure, the first element is the scanning and tracking head. It determines the line of sight by angles α_{T} and ε_{T} [6]. Next, these values and the angular displacement values are transmitted to the compensator block. In this block, new values of the targeting line angles θ_1^{zad} and θ_2^{zad} are calculated, compensating the motion of the artillery-missile system's base, which will be discussed in greater detail later in the paper.

At the same time, angles θ_1^{zad} and θ_2^{zad} are desired signals for the traverse and elevation systems. Subsequently, after calculating the azimuth control error e_1 and elevation control error e_2, the controllers calculate the control values u_1 and u_2.

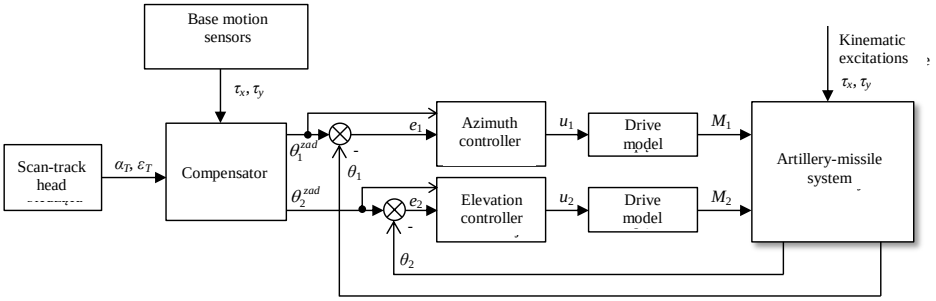

Fig. 3. Block diagram of control loop

Further blocks in the system are execution system models. These take into account the reducer gear ratio ($n_1 = 53\eta$ and $n_2 = 38\eta$, respectively, for azimuth and elevation systems, with efficiency of $\eta = 98\%$) as well as the limited torque generated on the motor shaft, which for the assumed SBL 4-0530 brushless motors is ±21 Nm [7]. Furthermore, drive dynamics were modelled using a first-order inertial term with a time constant $T = 0.02$ s. This represents the fact the driving torque cannot change discretely, which stems, for example, from the limited duration of current increase in the drive's winding.

The control moments M_1 and M_2 generated at gear reducer output affect the artillery-missile system's traverse and elevation movements. The system model takes into account the effects of internal disturbances (from firing the weapons) and the external disturbances affecting the base, in the form of kinematic inputs which generate additional forces that increase the difficulty in maintaining a desired trajectory during operation.

3.2. Control law

A key element of automatic control systems is the controller, which determines the dynamic properties of the entire system. In this case, i.e. controlling a artillery-missile (AM) system, the most important criterion is tracking a specific trajectory as precisely as possible, even under the influence of various disturbances. In this consideration, computed torque control – an inverse dynamics based solution is proposed, combined with PID controllers. Papers on this subject, for instance [8], indicate that this method is typically used for industrial robots and manipulators.

Here, the methods are implemented for an artillery system with additional correction components. The general control law for azimuth (5) and elevation (6) is defined as follows.

$$u_1 = u_1^{\mathrm{PID}} + k_1 u_1^{\mathrm{DO}} \tag{4}$$

$$u_2 = u_2^{\mathrm{PID}} + k_2 u_2^{\mathrm{DO}} + S \tag{5}$$

where: u_1, u_2 – total control values transmitted to servomotors, u_1^{PID}, u_2^{PID} – control values calculated by PID controllers, u_1^{DO}, u_2^{DO} – control values calculated using inverse dynamics, k_1, k_2 weight coefficients, S – corrective function depending on known dynamic disturbances.

The assumed PID controllers have a so-called independent structure and are formulated as $u_i^{\mathrm{PID}} = K_{Pi} e_i + K_{Ii} \int e\, dt + K_{Di} \dot{e}, (i = 1, 2)$. Initial PID controller parameters were calculated using the numerical optimisation described in [9].

After adjusting the parameters to improve control dynamics at the cost of minor overregulation in the interim (initial) motion phase, the parameters ultimately take the following forms: K_{P1} = 19.81; K_{I1} = 0; K_{D1} = 3.31 and K_{P2} = 9.23; K_{I2} = 4.16; K_{D2} = 0.95.

The u_1^{DO}, u_2^{DO} control values dependent on inverse dynamics are defined by equations (6) and (7), and arise out of the mathematical model of the GM system.

$$\begin{aligned} u_1^{DO} = {} & \left(3a\theta_2^2 + 2b\theta_2 + c\right)\dot{\theta}_1\dot{\theta}_2 + \left(I_1 + pn + q + a\theta_2^3 + b\theta_2^2 + c\theta_2 + d\right)\ddot{\theta}_1 \\ & + t_{11}\dot{\theta}_1^3 + t_{12}\dot{\theta}_1 \end{aligned} \tag{6}$$

$$\begin{aligned} u_2^{DO} = {} & I_2\left(\ddot{\theta}_2 + \ddot{\tau}_x \sin\theta_1 + \ddot{\tau}_y \cos\theta_1\right) - \frac{1}{2}\left(3a\theta_2^2 + 2b\theta_2 + c\right)\dot{\theta}_1^2 \\ & - mrg\cos\left(\theta_2 + \gamma + \tau_x \sin\theta_1 + \tau_y \cos\theta_1\right) + t_{21}\dot{\theta}_2^3 + t_{22}\dot{\theta}_2 \end{aligned} \tag{7}$$

The weight coefficients k_i introduced in equations (4) and (5) are intended to limit the impact of computed torque control in the event that the system's condition is inconsistent with a reference trajectory. In other words, when the system is far from a desired operating point, PID controllers play the primary role. When the operating trajectory is identical or close to a desired trajectory, computed torque control takes over, while PID controllers are auxiliary.

For the considered case, a corrective function in the form of a normal distribution with a mean value $\mu = 0$ and standard deviation $\sigma = 0.5$ degree, i.e. $k_i = \exp\left(\frac{-e_i}{2 \cdot 0{,}5^2}\right)$, was introduced. A graphical illustration of the weight coefficient function chart is shown in Fig. 4. The corrective function *S*, shown in equation (5), may be classified as feedforward auxiliary control. As tests have demonstrated, the elevation system is particularly sensitive to the dynamic impact inputs related to firing. It was therefore beneficial to introduce from the start a specific correction *S*, forming a saw-shaped drive moment impulse with a set peak value of -1000 Nm (recoil compensation) and duration of $t_S = 0.035$ s, triggered at the moment of firing.

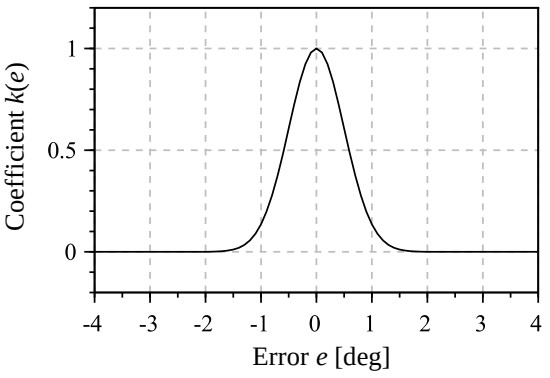

Fig. 4. Weight coefficient value as function of tracking error

3.3. Calculating aiming line correction

In the discussion in this paper it was assumed that the artillery-missile system is installed on a ship, and as a consequence of the impacts of sea waves, it is subjected – together with the ship – to displacement by angles τ_x, τ_y, as shown in the diagram in Fig. 5. As a result of these kinematic inputs (disturbances), the aiming line is no longer identical to the target observation line. Thus, it is necessary to compensate for the effects of sea waves, which translate to the motion of the base, for instance, by correcting the desired azimuth and elevation signals so that the effects of base motion on the displacement of the aiming line is compensated.

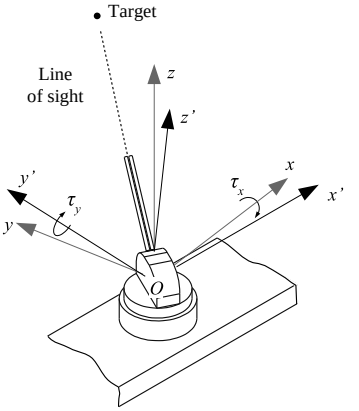

Fig. 5. Assumed system's base rotations

Azimuth and elevation corrections are calculated as follows. Fig. 6a shows the target, indicated by vector $\mathbf{v}_T$ in an unmoving coordinate system *Oxyz*. At the origin of coordinates *O*, there is the AM system aimed at the target defined by polar coordinates α_T and ε_T. The effects of sea waves have resulted in the AM system moving to point *O'*, which becomes the origin of coordinates for a moving coordinate system *O'x'y'z'* bound to the AM system, as shown in Fig. 6b. In order to continue tracking the target, the AM system must calculate a new angular position in traverse and elevation, defined by angles α_T^c i ε_T^c.

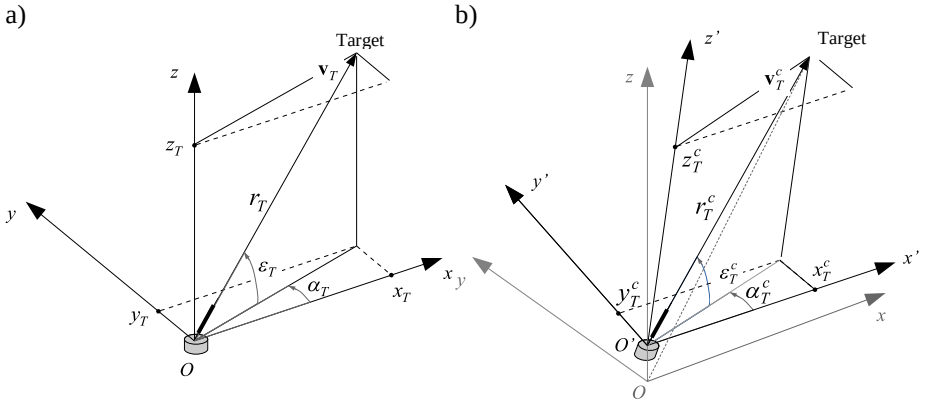

Fig. 6. Target coordinates in the a) unmoving and b) moving coordinate system

To determine angles α_T^c i ε_T^c, the target's polar coordinates α_T and ε_T and r_T were first transformed into Cartesian coordinates using equations:

$$x_T = r_T \cos\varepsilon_T \cos\alpha_T \tag{8}$$

$$y_T = r_T \cos\varepsilon_T \sin\alpha_T \tag{9}$$

$$z_T = r_T \sin\varepsilon_T \tag{10}$$

Next, Cartesian coordinates in the *Oxyz* were formulated as vector $\mathbf{v}_T = [x_T\ y_T\ z_T]^T$. The new vector $\mathbf{v}_T^c$ indicating the target in the displaced coordinate system is expressed in equation (11).

$$\mathbf{v}_T^c = \mathbf{R}_x\mathbf{R}_y\left(\mathbf{v}_T - \mathbf{T}\right) = \mathbf{R}_{xy}\left(\mathbf{v}_T - \mathbf{T}\right) \tag{11}$$

Where $\mathbf{R}_x$ and $\mathbf{R}_y$ are rotation matrices, and $\mathbf{T}$ is the translation vector. For the case in question, as in Fig. 5, the resulting rotation matrix $\mathbf{R}_{xy}$ takes form (12), while the translation vector is $\mathbf{T} = [0\ 0\ 0]^T$.

$$\mathbf{R}_{xy} = \begin{bmatrix} \cos\tau_y & 0 & -\sin\tau_y \\ \sin\tau_x\sin\tau_y & \cos\tau_x & \sin\tau_x\cos\tau_y \\ \cos\tau_x\sin\tau_y & -\sin\tau_x & \cos\tau_x\cos\tau_y \end{bmatrix} \tag{12}$$

Returning to polar coordinates expressed in relation to the AM system's coordinate system is enabled by equations:

$$r_T^c = \sqrt{{x_T^c}^2 + {y_T^c}^2 + {z_T^c}^2} \tag{16}$$

$$\varepsilon_T^c = \arcsin\frac{z_T^c}{r_T^c} \tag{17}$$

$$\alpha_T^c = \arctan\frac{y_T^c}{x_T^c} \tag{18}$$

Ultimately, it can be specified that desired control angles must equal target observation angles in the displaced system *O'x'y'z'*, meaning $\theta_1^{zad} = \alpha_T^c$ and $\theta_2^{zad} = \varepsilon_T^c$. As an example, input disturbances τ_x, τ_y shown in Fig. 7 were generated, whose nature is similar to the ship's rocking and swaying signals shown in [10].

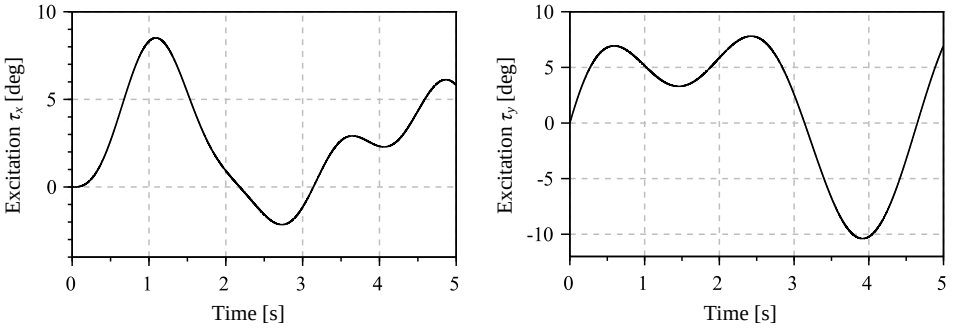

a) b)

Fig. 7. Generated waveforms of kinematic disturbances a) τ_x and b) τ_y

Fig. 8 shows sample target observation charts in the traverse and elevation systems, including trajectories compensating the interference discussed.

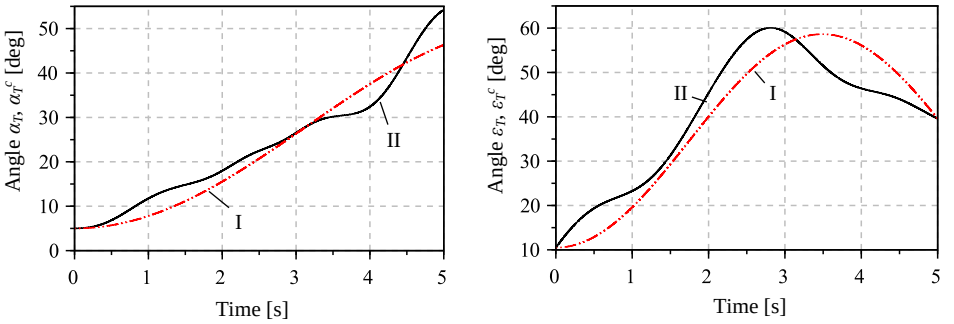

a) b)

Fig. 8. Original (I) and compensated (II) trajectories for a) azimuth and b) elevation angles

4. EXAMPLE OF CONTROL SIMULATION

4.1. Assumptions

In the simulation example presented, the desired signals for the AM system's control system are compensation trajectories from Fig. 8, which represent tracking of a manoeuvring aerial target while the AM system's base is affected by kinematic interference. It was assumed that the AM system's initial position is different from the desired position. An important issue from the perspective of control was that identification uncertainty of the object of control should be taken into account. It was assumed that the object of control is not identical to the inverse dynamics model implemented in the regulator. It was assumed that compared to the model, the object of control has: 40% greater turret moment of inertia and 25% greater gun cradle moment of inertia, gun cradle mass is 10% greater, and the friction generated in the system is 30% greater.

In the simulation, dynamic disturbances from firing takes the form of saw-shaped moment impulses with an estimated value of 12,000 Nm and duration of 0.0019 s. This disturbances unilaterally affects the elevation system and alternately affects the azimuth system. A burst of 15 bullets every 0.15 s begins on second 1.5 of the simulation, when the AM system is sufficiently accurately aimed at the set trajectory.

4.2. Results of control

Fig. 9 shows the simulation results of controlling the AM system using the proposed computed torque control for the case in question. As indicated by the charts generated, the trajectory compensating the kinematic interference is implemented correctly. There are no clear target tracking errors or signs of control system instability visible in the charts shown.

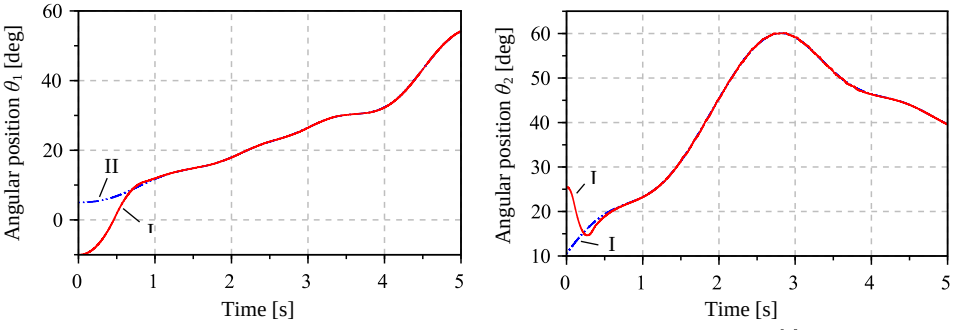

a) b)

Fig. 9. Performed (I) and desired (II) position in a) azimuth and b) elevation

Fig. 10 shows the azimuth and elevation angular velocities for the motion performed. The first adjustment phase of the motion can be identified in the charts, where the highest velocities are achieved. The effects of dynamic interference from firing also manifest, particularly clear for the elevation system due to the relatively lower gun cradle inertia. Compensation of kinematic interference manifests as curve modulation.

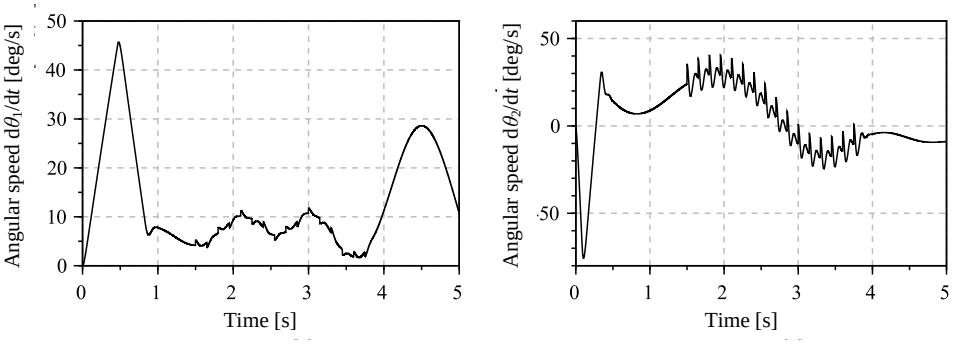

a) b)

Fig. 10. Angular speed graphs for a) azimuth and b) elevation motion

Fig. 11 shows drive moments generated when executing the motion. Here, the phenomenon of drive saturation and a clear effort by the execution systems to compensate the firing interference are noticeable, as before, particularly for the elevation system.

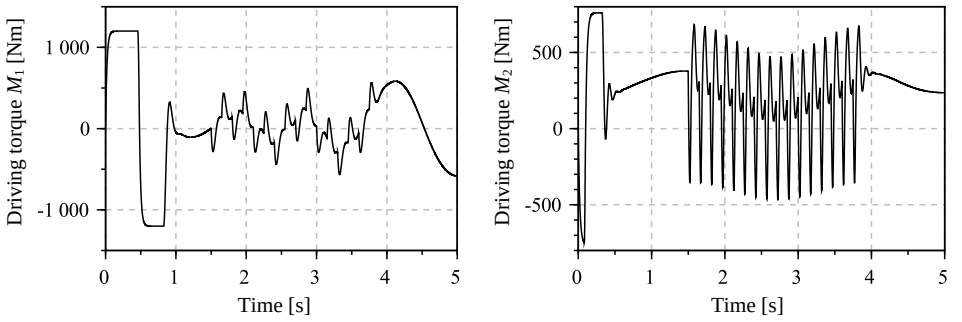

a) b)

Fig. 11. Driving torques acting on a) azimuth and b) elevation system

Motion trajectories desired and performed by the system are shown in Fig. 12. Due to kinematic disturbances, the motion trajectory required to track the target is highly deformed. The figure also shows a magnified fragment of the chart, where recoil and a certain inaccuracy of executing the trajectory are visible in the moments following individual shots.

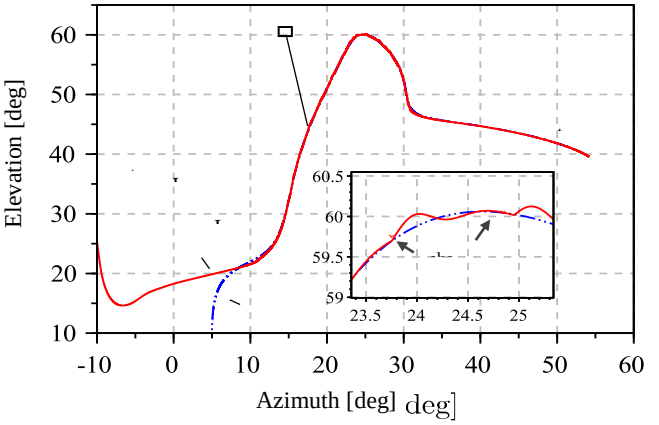

Fig. 12. Performed (I) and desired (II) trajectory in spherical coordinates

4.3. Analysis of control error

In order to visually analyse the precision of control and execution of desired trajectories, control error graphs for azimuth and elevation are shown in Fig. 13, with scales chosen so that minor errors are visible. For comparison, graphs generated from two simulations differing in the regulators used are shown in the figures. In the first case, regulators based on modified inverse dynamics were used, in the second one, only PID regulators were used for control.

It is clearly visible that the use of inverse dynamics provides more precise target tracking and, after the interim period, the maximum error does not exceed 0.1 degree in azimuth and 0.22 degree in elevation. It must be noted that at the moments of firing, the error is lower and it takes on the maximum value after the bullet leaves the barrel.

Table 1 summarises the values of performance indices for both simulations. IAE (integral of absolute error) and ISE (integral of square error) were calculated for the simulation time section from 1.5 s to 5 s in order to only take the target tracking process into account.

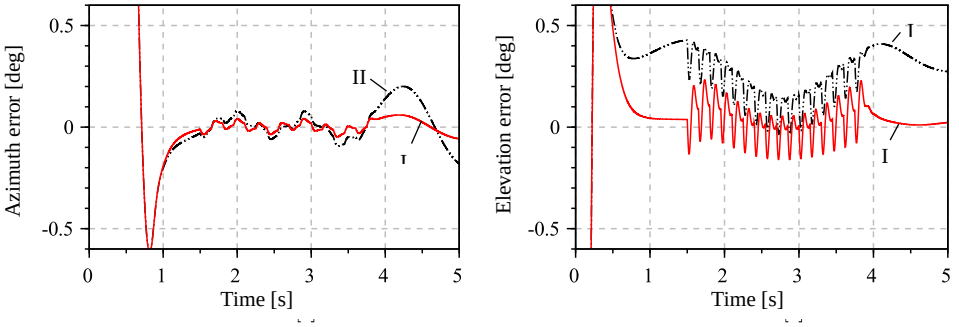

a) b)

Fig. 13. Tracking errors for modified CTC (I) and PID (II) controllers for a) azimuth and b) elevation

Table 1. Performance indices for different controllers

Controller type	Azimuth		Elevation	
	IAE	ISE	IAE	ISE
Mod. inv. dynamics	0.010420	0.000107	0.0373055	0.0013917
PID	0.030007	0.000900	0.4276615	0.1828944

5. SUMMARY AND CONCLUSIONS

The paper demonstrates that the proposed control method using modified inverse dynamics enables fairly precise target tracking in spite of the AM system being affected by dynamic and kinematic disturbances, and in spite of the differences between the dynamics model and the object of control, introduced on purpose. The use of the weight coefficient additionally enabled maintaining the system's stability when the system is far from the desired operating position. This method noticeably improves control quality compared to PID regulators, in particular for position control in the elevation system.

A certain inconvenience of the method in question is the necessity to know the derivatives of the desired system state, which under actual conditions may require additional signal estimation and/or filtering, e.g. using a Kalman filter or differential filters. The test computer (Intel i3 4000M CPU, 8 GB RAM) made it possible, at integration setup $dt = 0.0002$ s, to perform the control calculations in real time.

REFERENCES

[1] Gacek Józef, Jacek Gwardecki, Jan W. Kobierski, Zbigniew Leciejewski, Sławomir Łuszczak, Stanisław Milewski, Tadeusz Świętek, Ryszard Woźniak, Zbigniew Wójcik. 2016. Structure and innovative technologies in the new Polish 35 mm naval weapon system. In *Materiały konferencyjne XI Międzynarodowej Konferencji Uzbrojeniowej "Naukowe aspekty techniki uzbrojenia i bezpieczeństwa"*, str. 246-247. Warszawa: Wydawnictwo Wojskowej Akademii Technicznej w Warszawie

[2] http://www.defence24.pl/292995,fbm-armata-35-mm-tryton-dla-kormorana (2018)

[3] https://www.defence24.pl/dialog-na-morska-armate-23-mm (2018)

[4] Zakłady Mechaniczne Tarnów, http://www.zmt.tarnow.pl/wordpress/item/23mm-przeciwlotniczy-morski-zestaw-artyleryjsko-rakietowy-zu-23-2mr/ (2018)

[5] Szmidt Piotr. 2017. "A compensation for positioning of the remote control artillery-missile set in external disturbance conditions". *Vibration, Control and Stability of Dynamical Systems* 23 : 513-524.

[6] Gapiński Daniel. 2016. Zmodyfikowana optyczna głowica skanująco-śledząca jako układ do poszukiwania, identyfikacji i śledzenia celów powietrznych. *Rozprawa doktorska.* Kielce: Wydawnictwo Politechniki Świętokrzyskiej w Kielcach

[7] SBL/K Motor Catalogue, http://docplayer.net/5976825-Sbl-k-motor-catalogue-2002.html (2018)

[8] Pereira Aaron, Matthisa Althoff. 2015. Safety control of robots under Computed Torque control using reachable sets. In *Proceedings - IEEE International Conference on Robotics and Automation* 331-338.

[9] Koruba Zbigniew, Daniel Gapiński, Piotr Szmidt. 2017. The analysis of optimal PID controllers parameters selection for missile-artillery system. In *Proceedings of the 23rd International Conference on Engineering Mechanics* 970-973. 15 - 18 May 2017, Svratka, Czech Republic.

[10] Wełnicki Wiesław. 1989. *Mechanika ruchu okrętu*. Gdańsk: Wydawnictwo Politechniki Gdańskiej.

Sterowanie zestawem artyleryjsko-rakietowym w warunkach występowania zakłóceń za pomocą zmodyfikowanej metody opartej o dynamikę odwrotną

Piotr SZMIDT

Wydział Mechatroniki i Budowy Maszyn, Politechnika Świętokrzyska
al. Tysiąclecia Państwa Polskiego 7, 25-314, Kielce

Streszczenie. W pracy zajęto się zagadnieniem sterowania zdalnie sterowanym zestawem artyleryjsko-rakietowym w warunkach oddziaływania na zestaw zakłóceń dynamicznych i kinematycznych. Do analizowanych w artykule zakłóceń dynamicznych należy zaliczyć zakłócenia pochodzące od strzałów, zaś zakłócenia kinematyczne stanowią zakłócenia związane z ruchem podstawy, na której posadowiony jest zestaw. Obiekt badań stanowi model zestawu oparty o stosowany i produkowany w Polsce zestaw artyleryjsko-rakietowy typu ZU-23-2MR, który przeznaczony jest do zwalczania lekko opancerzonych celów powietrznych, nawodnych i lądowych .Po omówieniu modelu zestawu jak i modelu przyjętych zakłóceń, w dalszej części pracy poddano analizie układ sterowania położenia kątowego w azymucie i elewacji wyżej wymienionego zestawu. Przedstawiono sterowanie oparte o metodę dynamiki odwrotnej z dodatkowymi członami korygującymi. Przyjęto także pewną inercję w modelach napędu układów. Dodatkowo, założono niepewność identyfikacji modelu, tj. parametry obiektu sterowania są różnie od parametrów modelu, który stanowi podstawę do obliczenia wartości sterujących.
Uwzględniono przy tym różnicę w masach, masowych momentach bezwładności oraz momentach tarcia powstających w układach napędowych zestawu. Ostatnia część pracy obejmuje analizę szybkości przechwycenia i dokładności śledzenia manewrującego celu powietrznego przy działających na zestaw zakłóceniach. Założono, że zestaw znajduje się na okręcie, pojawiają się zatem zakłócenia kinematyczne związane z ruchem okrętu na fali morskiej, a także zakłócenia dynamiczne wynikające z oddawania strzałów.
Wszystkie symulacje zostały przeprowadzone w środowisku Scilab i dla nieliniowego modelu zestawu. Najistotniejsze wyniki przedstawiono w postaci graficznej.
Słowa kluczowe: automatyka i robotyka, sterowanie, zestaw artyleryjsko-rakietowy, dynamika odwrotna, zakłócenia